

Groundwater pumping impacts on real stream networks: testing the performance of simple management tools

Authors: Samuel C. Zipper^{1,2,*}, Tom Dallemagne¹, Tom Gleeson¹, Thomas C. Boerman¹, Andreas Hartmann^{3,4}

Author Affiliations:

1. Department of Civil Engineering, University of Victoria, Victoria BC, Canada

2. Department of Earth & Planetary Sciences, McGill University, Montreal QC, Canada

3. Institute of Earth and Environmental Sciences, University of Freiburg, Germany

4. Department of Civil Engineering, University of Bristol, United Kingdom

*Corresponding author: zipper@uvic.ca; +1-206-909-1277; PO Box 1700, Stn CSC, Victoria BC V8W 2Y2, Canada

Author ORCiDs:

SCZ: 0000-0002-8735-5757

TD: N/A

TG: 0000-0001-9493-7707

TCB: 0000-0001-9508-0661

AH: 0000-0003-0407-742X

Index Terms: 1830 Groundwater/surface water interaction; 1894 Instruments and techniques: modeling; 1842 Irrigation; 1834 Human impacts; 1880 Water management

Key Points (≤ 140 characters):

- New streamflow depletion apportionment equation with stream geometry performs best across a variety of stream network geometries
- Performance of all depletion apportionment equations decreases with increased drainage density, elevation, and groundwater recharge rates
- Spatial application of Kling-Gupta Efficiency is useful for identifying different sources of error and accompanying management implications

29 **Abstract**

30 Quantifying reductions in streamflow due to groundwater pumping ('streamflow depletion') is
31 essential for conjunctive management of groundwater and surface water resources. Analytical
32 models are widely used to estimate streamflow depletion but include potentially problematic
33 assumptions such as simplified stream-aquifer geometry and rely on largely untested depletion
34 apportionment equations to distribute depletion from a well among different stream reaches.
35 Here, we use archetypal numerical models to evaluate the sensitivity of five depletion
36 apportionment equations to stream networks with varying drainage densities, topographic relief,
37 and recharge rates; and statistically evaluate the sources of error for each equation. We introduce
38 a new depletion apportionment equation called web squared which considers stream network
39 geometry, and find that it performs the best under most conditions tested. For all depletion
40 apportionment equations, performance decreases with increases in drainage density, relief, or
41 groundwater recharge rates, and all equations struggle to estimate depletion in short stream
42 reaches. Poorly performing apportionment equations tend to underestimate streamflow depletion
43 relative to numerical model results, leading to a negative bias and underpredicted variability,
44 while error in the best performing apportionment equations tends to be due to imperfect
45 correlation. From a management perspective, equations with error primarily due to bias and
46 variability are preferable as they identify which reaches will be affected and can be statistically
47 corrected. Overall, these results indicate that the web squared method introduced here, which
48 explicitly considers stream geometry, performs the best over a range of real-world conditions,
49 and will be most accurate in flatter and drier environments.

50 **Plain Language Summary**

51 Pumping groundwater for human uses such as irrigation can reduce flow in nearby streams by
52 intercepting water which otherwise would have eventually flowed into the river channel. This
53 'streamflow depletion' reduces the water available to downstream users and aquatic ecosystems.
54 Due to a lack of data and resources, relatively simple ('analytical') groundwater models are often
55 used to estimate the impacts of pumping, but they are based on several assumptions, such as
56 linear streams. In this study, we introduce a new 'depletion apportionment' equation used to
57 estimate pumping impacts that considers the spatial complexity of real stream networks. By
58 comparing it to more complex ('numerical') groundwater models, we find that our new equation
59 works better than existing equations under a wide variety of conditions. Furthermore, all of the
60 depletion apportionment equations we test perform best in flatter, drier settings where streams
61 are spaced further apart. Finally, we compare the different causes of error for different depletion
62 apportionment equations, which have different implications for water management decisions.
63 Overall, our results show that stream geometry is an important factor to consider when making
64 decisions about groundwater pumping, and the new depletion apportionment equation introduced
65 here is a useful new tool for water managers.

66 **Keywords:** groundwater-surface water interactions; streamflow depletion; groundwater
67 pumping; groundwater models; depletion apportionment; environmental flows;

68 **1 Introduction**

69 Groundwater is a critical contributor to streamflow and supports both aquatic ecosystems
70 and human needs (Acreman et al., 2014; Booth et al., 2016; Gleeson & Richter, 2017; Zektser et
71 al., 2005). For instance, groundwater discharge into streams provides a stable supply of water
72 during dry periods and is a key regulator of water temperature, an important water quality
73 parameter for aquatic ecosystems (Johnson et al., 2017; Kurylyk et al., 2014, 2015; Strauch et al.,
74 2017; Zorn et al., 2012). It has long been recognized that groundwater pumping can reduce
75 streamflow via the interception of groundwater that would have otherwise discharged into a
76 stream (Bredehoeft et al., 1982; Bredehoeft, 2002; Theis, 1941). In extreme cases, pumping may
77 even reverse the hydraulic gradient at the stream and induce infiltration from the streambed into
78 the aquifer (Barlow & Leake, 2012). Reductions in groundwater discharge to and/or induced
79 infiltration from streams are broadly known as ‘streamflow depletion’, and can have devastating
80 effects on ecosystems and downstream water users (Barlow & Leake, 2012; Zorn et al., 2012).

81 Streamflow depletion is not possible to measure directly and can be quantified using both
82 numerical and analytical models. Numerical models (e.g. MODFLOW) are widely used for the
83 evaluation of pumping impacts on groundwater levels and discharge to streams (Ahlfeld et al.,
84 2016; Bredehoeft & Kendy, 2008; Lackey et al., 2015). However, numerical models are time-
85 and labor-intensive to construct, validate, and apply (Rathfelder, 2016). Therefore, they are
86 typically generated for a specific aquifer and used at local to regional scales (Leake et al., 2010;
87 Nyholm et al., 2002).

88 On the other hand, analytical models of streamflow depletion have the advantage of being
89 computationally simple, and are therefore often used for water management and permitting
90 decisions (Jayawan et al., 2016; Miller et al., 2007; Reeves et al., 2009). However, analytical
91 solutions adopt a suite of assumptions often including that of an infinite horizontal aquifer
92 bounded by a single linear stream (Glover & Balmer, 1954; Hantush, 1965; Hunt, 1999; Jenkins,
93 1968; Theis, 1941). Several studies have evaluated the performance of different analytical
94 models via comparison with numerical models, and found that resistance to flow through the
95 streambed (Jayawan et al., 2016; Sophocleous et al., 1995); subsurface heterogeneity and
96 anisotropy (Li et al., 2016); aquifer storativity (Jayawan et al., 2016); and the degree of aquifer
97 penetration by the stream channel (Butler et al., 2001; Sophocleous et al., 1995) are particularly
98 important considerations.

99 To use analytical models in real-world settings, geometric methods known as ‘depletion
100 apportionment’ equations are used to distribute streamflow depletion calculated analytically for a
101 single reach to stream networks with multiple reaches. However, relatively little research has
102 compared the performance of different depletion apportionment equations. Reeves et al. (2009),
103 the only study the authors are aware of, evaluated nine depletion apportionment equations via
104 comparison with output from a MODFLOW numerical model during the development of the
105 Michigan Water Withdrawal Assessment Tool (<http://www.deq.state.mi.us/wwat>). They elected
106 to use an inverse-distance weighting approach (described in more detail in Section 2.2) in their
107 tool because it performed reasonably well compared to numerical model output, was relatively
108 simple to calculate, and has a theoretical basis in analytical solutions to streamflow depletion

109 with multiple streams (Wilson, 1993). However, this comparison was based on a single
110 watershed within a larger regional-scale groundwater flow model, and therefore the
111 transferability of their conclusions to stream networks with different hydrological characteristics
112 (for example, drainage density, topographic relief, and groundwater recharge) is unknown.

113 To enhance the utility of analytical models as a management tool, we ask, *which*
114 *depletion apportionment equations compare most favorably to numerical model simulations*
115 *across a range of realistic stream networks?* Using the groundwater flow system around
116 Nanaimo, British Columbia (Canada) as an exemplar, we test a suite of analytical depletion
117 apportionment methods across stream networks varying in drainage density, topographic relief
118 and recharge flux. We make three novel contributions to the literature: (1) the introduction of
119 two new depletion apportionment equations, which we call web and web squared (Section 2.2);
120 (2) a novel spatial application of model evaluation criteria typically used for timeseries data
121 (Section 2.4) and the development of new visualization methods to assess sources of error
122 (Sections 3.1 and 4.2); and (3) evaluation and sensitivity analysis of five depletion
123 apportionment equations across diverse stream network geometries (Sections 3.1-3.3) to guide
124 their use in water resource management.

125 **2 Methods**

126 **2.1 Modeling approach**

127 Modeling approaches to quantify streamflow depletion within a stream network can be
128 broadly divided into three groups (Table 1): (1) analytical models paired with depletion
129 apportionment equations; (2) archetypal numerical models which simplify real-world conditions
130 to evaluate processes in a generalizable manner; and (3) site-specific numerical models. The
131 choice of approach depends on the aims of a particular study, and the modeler must weigh trade-
132 offs between complexity, available resources, and intended model application. For water
133 resource management, analytical solutions are often used for preliminary analysis and in data-
134 scarce settings due to the relative simplicity of developing and implementing them. As resources
135 and interest are available, analytical models are often superseded by site-specific numerical
136 models, which allow for detailed exploration of different management strategies on local surface
137 water-groundwater interactions.

138 In this study, our goal was to evaluate the sensitivity of depletion apportionment equation
139 performance to different stream network geometries by systematically varying drainage density,
140 topographic relief, and groundwater recharge rates. Thus, we elected to use archetypal numerical
141 models for comparison to eliminate local, site-specific complexity and instead focus on process-
142 based understanding (Gleeson et al., 2016; Voss, 2011a, 2011b; Zipper et al., 2017). Archetypal
143 models use a realistic set of hydraulic parameters to provide broadly relevant output, and are
144 therefore not calibrated as they are not intended to recreate real-world conditions. This approach
145 allows us to isolate the impacts of stream network geometry on streamflow depletion and answer
146 the question posed in Section 1. Furthermore, we are not testing the performance of one or
147 multiple analytical models, as has been accomplished in previous work (Butler et al., 2001;
148 Jayawan et al., 2016; Li et al., 2016; Sophocleous et al., 1995; Spalding & Khaleel, 1991).
149 Rather, we are comparing the distribution of depletion within a stream network among various

150 depletion apportionment equations (Section 2.2) with our archetypal numerical model (Section
 151 2.3).

152 **Table 1.** Comparison of streamflow depletion modeling approaches.

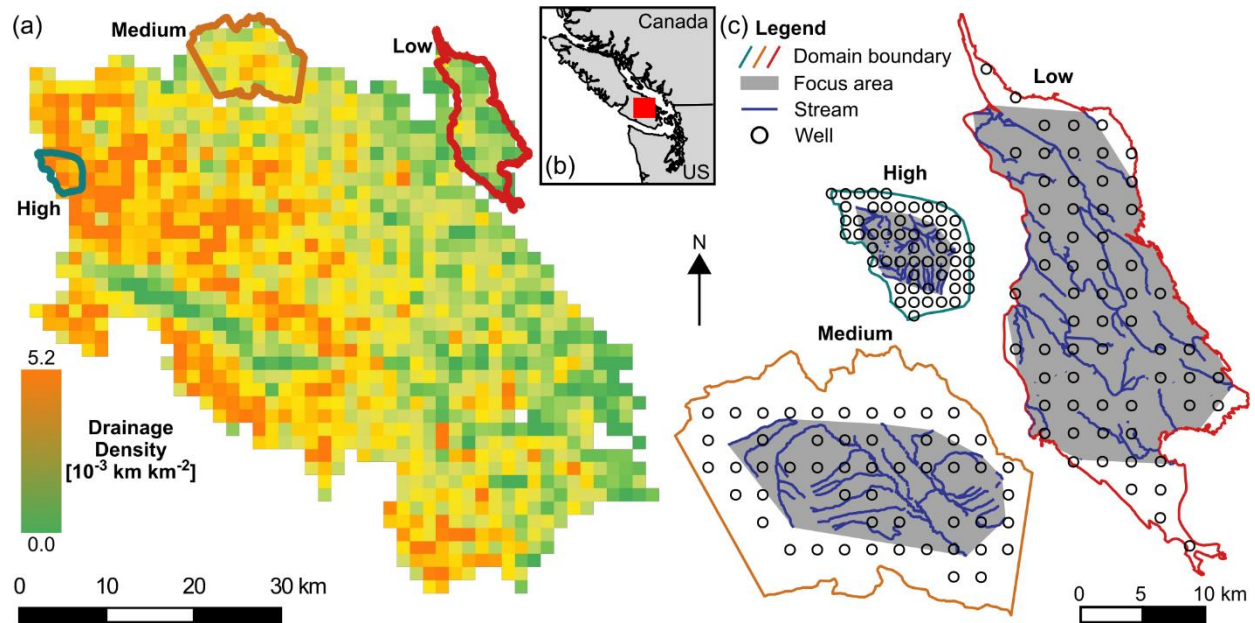
	Analytical models with apportionment equations	Archetypal numerical models	Site-specific numerical models
Boundary conditions	Analytical models consider one or two streams with simplified geometry and constant head; depletion apportionment equations distribute depletion to different stream reaches.	Complex stream geometry simulated as constant river boundary condition with specified head.	Complex stream geometry represented by a mix of boundary conditions such as river, constant head, drain etc.
Parameter values, input data and geometry	Analytical models assume flat, infinite homogeneous, isotropic aquifers with no vertical flow. Input data datasets exist for most aquifers.	Homogeneous and isotropic aquifer; topographic relief can be included. Moderate input data requirements which exist for most aquifers.	Heterogeneous and anisotropic, multiple layers with complex geometry. Many regions do not have enough data.
Required effort, skill and calibration	Moderate effort (minutes - days) and skill (generalists). Not calibrated.	Significant effort (weeks) and skill (specialists). Not calibrated.	Significant effort (months) and skill (experts). Calibrated to hydrogeologic and hydrologic measurements.
Examples from literature	Foglia et al., 2013; Jayawan et al., 2016; Reeves et al., 2009. Only Reeves tested depletion apportionment equations.	Kendy & Bredehoeft, 2006; Konikow & Leake, 2014; Lackey et al., 2015.	Ahlfeld et al., 2016; Feinstein et al., 2016; Fienen et al., 2018; Reeves et al., 2009.

153

154 Our archetypal domain was based on the groundwater system around the City of
 155 Nanaimo on Vancouver Island, British Columbia, Canada (Figure 1). We selected this domain
 156 due to a strong east-west gradient in drainage density, calculated as the length of stream per
 157 1500- m spatial resolution grid cell. We took advantage of this natural gradient by selecting three
 158 subdomains corresponding to low, medium, and high drainage density for testing the
 159 apportionment equations (Figure 1). Each of these domains has 62 stream reaches, but vary in
 160 area from 7.6 km² (high density) to 81.6 km² (low density). Stream network geometry are from
 161 the Canadian National Hydro Network (Government of Canada, 2016).

162 To test the depletion apportionment equations, we created a grid of synthetic pumping
 163 wells in each drainage density domain, the spacing of which varied between drainage densities
 164 due to the order of magnitude difference in domain size. After creating the grid, we eliminated
 165 wells in MODFLOW cells which contained a river segment (see Section 2.3 for more details
 166 about the MODFLOW model). This led to slight differences in the total number of wells between
 167 the domains, though all had at least 50 pumping wells. In the low density domain, there were 62

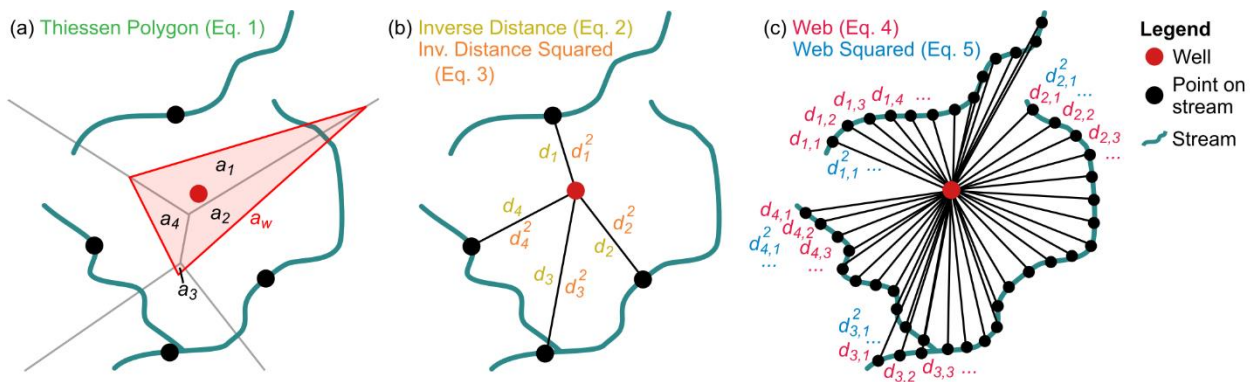
168 wells spaced at 1080 m; in the medium density domain, there were 52 wells spaced at 1009 m;
 169 and in the high density domain, there were 54 wells spaced at 494 m (Figure 1c).



170
 171 **Figure 1.** (a) Drainage density map of Nanaimo Aquifer and (b) location of Nanaimo Aquifer on
 172 Vancouver Island, Canada; red square shows (a). Colored outlines in (a) are locations of high, medium,
 173 and low drainage density focus domains shown in (c).

174 2.2 Depletion apportionment equations

175 To evaluate different apportionment equations, we calculated the streamflow depletion
 176 fraction for each stream reach while pumping each well using five different apportionment
 177 equations (Figure 2). The first three (Thiessen polygon, inverse distance, and inverse distance
 178 squared) were previously evaluated in Reeves et al. (2009) for the Kalamazoo aquifer in
 179 Michigan, while the final two (web inverse distance and web inverse distance squared)
 180 are new contributions in this study which are designed to consider the entire geometry of a stream
 181 network, rather than a single point on each stream reach.



182
 183 **Figure 2.** Diagrams showing (a) Thiessen polygon, (b) inverse distance, and (c) web inverse distance
 184 apportionment methods. Black dots in (a) and (b) are the points on the stream closest to the well. Letters
 185 correspond to variables in Equations 1-5.

186 The Thiessen polygon approach (Eq. 1) is an area-based approach which uses two sets of
 187 Thiessen polygons to weight streamflow depletion between stream reaches (Figure 2a). The first
 188 set of polygons is created using the point on each stream reach closest to the well of interest. The
 189 second set is created using the location of the well in addition to the point on each stream reach
 190 closest to the well. Streamflow depletion is then weighted based on the fraction of the well
 191 polygon from the second set which overlaps each stream reach polygon from the first set as
 192 follows:

$$f_i = \frac{a_i}{a_w} \quad \{\text{Eq. 1}\}$$

193 where

194 f_i = fraction of total depletion, Q_f , apportioned to stream reach i [-],

195 a_i = area of the first set of polygons contained within the well polygon in the second set
 196 of polygons [L^2], and

197 a_w = area of the well polygon in the second set of polygons [L^2].

198 The inverse distance (Eq. 2) and inverse distance squared (Eq. 3) approaches are based on
 199 the point on each stream reach with the shortest distance to the well of interest. We modify the
 200 approach of Reeves et al. (2009) slightly to include the distance to all stream reaches in the
 201 model domain, rather than just those in neighboring catchments (Figure 2b) in order to consider
 202 potential underflow of partially penetrating streams:

$$f_i = \frac{\frac{1}{d_i}}{\sum_{j=1,n} \frac{1}{d_j}} \quad \{\text{Eq. 2}\}$$

$$f_i = \frac{\frac{1}{d_i^2}}{\sum_{j=1,n} \frac{1}{d_j^2}} \quad \{\text{Eq. 3}\}$$

203 where

204 d = distance from the well to the closest point on stream reach j , and

205 n = total number of stream reaches.

206

207 The web (Eq. 4) and web squared (Eq. 5) approaches are similar to the inverse distance
 208 and inverse distance squared approaches, respectively, except they use the distance to a series of
 209 equally spaced (5 m in this study) points along all stream reaches in the domain, thus considering
 210 the length and geometry of each stream reach (Figure 2c):

$$f_i = \frac{\sum_{p=1, P_i} \frac{1}{d_{i,p}}}{\sum_{j=1, n} \left(\sum_{p=1, P_j} \frac{1}{d_{j,p}} \right)} \quad \{\text{Eq. 4}\}$$

$$f_i = \frac{\sum_{p=1, P_i} \frac{1}{d_{i,p}^2}}{\sum_{j=1, n} \left(\sum_{p=1, P_j} \frac{1}{d_{j,p}^2} \right)} \quad \{\text{Eq. 5}\}$$

211 where

212 P = total number of points on stream reach j , and

213 $d_{i,p}$ = distance from the well to point p .

214 We conducted exploratory analysis using a range of exponents for the inverse distance
 215 and web approaches in addition to squared (e.g. d^3 , d^4 , etc.), but elected to conduct our full
 216 analysis using only d and d^2 since higher exponents did not significantly improve performance
 217 and are less justified by hydrologic theory.

218 **2.3 Numerical modeling**

219 To evaluate the performance of the different analytical apportionment equations in a
 220 variety of stream network geometries, we performed a sensitivity analysis by comparing
 221 depletion apportionment equation results to archetypal numerical models parameterized with
 222 different drainage densities, topographic relief, and recharge rates. We selected these variables
 223 for sensitivity analysis because they exert a strong control on stream network geometry: drainage
 224 density by defining the spatial distribution of streams, topographic relief by changing the vertical
 225 position of both streams and pumping wells, and groundwater recharge by changing the water
 226 table geometry and the aquifer thickness. Given our focus on stream and aquifer geometry, we
 227 did not conduct a sensitivity analysis to the parameters controlling subsurface flow (e.g. Table
 228 2). Previous research has focused on this (Butler et al., 2001; Jayawan et al., 2016; Li et al.,
 229 2016; Sophocleous et al., 1995) and future work will investigate additional stream geometries
 230 under a wide range of subsurface parameterizations.

231 First, we tested sensitivity to drainage density by creating an archetypal steady-state
 232 numerical model of each drainage density domain using MODFLOW-2005 (Harbaugh, 2005), a
 233 finite-difference saturated groundwater flow model which has previously been used to evaluate
 234 the performance of analytical solutions of streamflow depletion (Butler et al., 2001; Jayawan et
 235 al., 2016; Reeves et al., 2009; Sophocleous et al., 1995). As discussed above (Section 2.1), these
 236 models were intended to be simplified representations of the Nanaimo Aquifer to isolate the
 237 impact of different stream geometries on streamflow depletion, rather than site-specific
 238 calibrated numerical models (Table 1).

239 Most parameters were constant across the three drainage density domains (Table 2), and
 240 selected to be representative of a typical sandy alluvial aquifer (Fetter, 2000). Each domain had a

241 flat land surface with an unconfined aquifer extending 100 m below ground for the initial
 242 simulations. Streams were represented using the river (RIV) package as 4 m in depth, 10 m in
 243 width, with a streambed thickness of 1 m and streambed conductivity of 0.01 m s^{-1} . We
 244 simulated pumping wells using the well (WEL) package. Wells were screened over the entire
 245 aquifer thickness (100 m) and pumped at a rate of $1000 \text{ m}^3 \text{ d}^{-1}$. We ignored the potential
 246 contributions of non-flowing surface water features; lakes within the domain were not
 247 considered, and the ocean (which is along the north edge of the medium density domain and all
 248 edges of the low density domain except the west) were set as inactive cells (no-flow) to avoid
 249 variable-density flow and contribution to pumping from ocean water, which was outside the
 250 scope of this study.

251 **Table 2.** Numerical MODFLOW model parameters.

Parameter	Value
<i>Number of rows x number of columns</i>	Low Density: 200 x 100 Medium Density: 105 x 135 High Density: 62 x 56
<i>Cell width x cell height</i>	Low Density: 107.3 m x 103.6 m Medium Density: 101.1 m x 100.9 m Low Density: 101.5 m x 100.4 m
<i>Number of layers</i>	10
<i>Layer thickness</i>	10 m
<i>Hydraulic conductivity (isotropic)</i>	$1 \times 10^{-5} \text{ m s}^{-1}$
<i>Specific Storage</i>	$1 \times 10^{-5} \text{ m}^{-1}$
<i>Specific Yield</i>	0.2
<i>Effective porosity</i>	0.14
<i>Total porosity</i>	0.3

252

253 Second, we conducted an additional sensitivity analysis of our depletion apportionment
 254 equations to topographic relief and groundwater recharge in the low density domain since this is
 255 domain had the best overall performance in the flat simulations (see Section 3.1) and thus should
 256 be more sensitive to changes than a poorly performing domain whose performance cannot
 257 decrease as much. First, we introduced relief into the domain using the Canada digital elevation
 258 model for the low density portion of the aquifer (Natural Resources Canada, 1997). The top of
 259 the numerical model domain was defined as the land surface, which ranged from 0 to 211 m
 260 above sea level [masl]. The top 9 layers were terrain-following and 10 m in thickness, and the
 261 bottommost layer extended to -100 masl. Wells were screened over their top 100 m. We then
 262 tested the effects of groundwater recharge over the low density domain with relief using the
 263 recharge (RCH) package. We applied 5 different recharge rates (0.01, 0.05, 0.1, 0.5, and 1.0 m
 264 yr^{-1}) to represent a range of recharge/hydraulic conductivity ratios (3.17×10^{-5} to 3.17×10^{-3}). To

265 compensate for the increased supply of water, we also increased the pumping rate to 5000 m³ d⁻¹.
266 All other parameters were the same as the flat low density model.

267 To calculate streamflow depletion from the numerical model (Eq. 6), we used the zone
268 budget feature of MODFLOW to define each stream reach within our input hydrography dataset
269 as a zone. We then ran a steady-state simulation with no pumping, and simulations turning on
270 each well one-at-a-time. Streamflow depletion for each zone was the difference in water
271 exchange between the zone and the rest of the domain relative to the no-pumping simulation, and
272 divided that by the cumulative difference in water exchange across all stream reaches to estimate
273 the streamflow depletion fraction for each well:

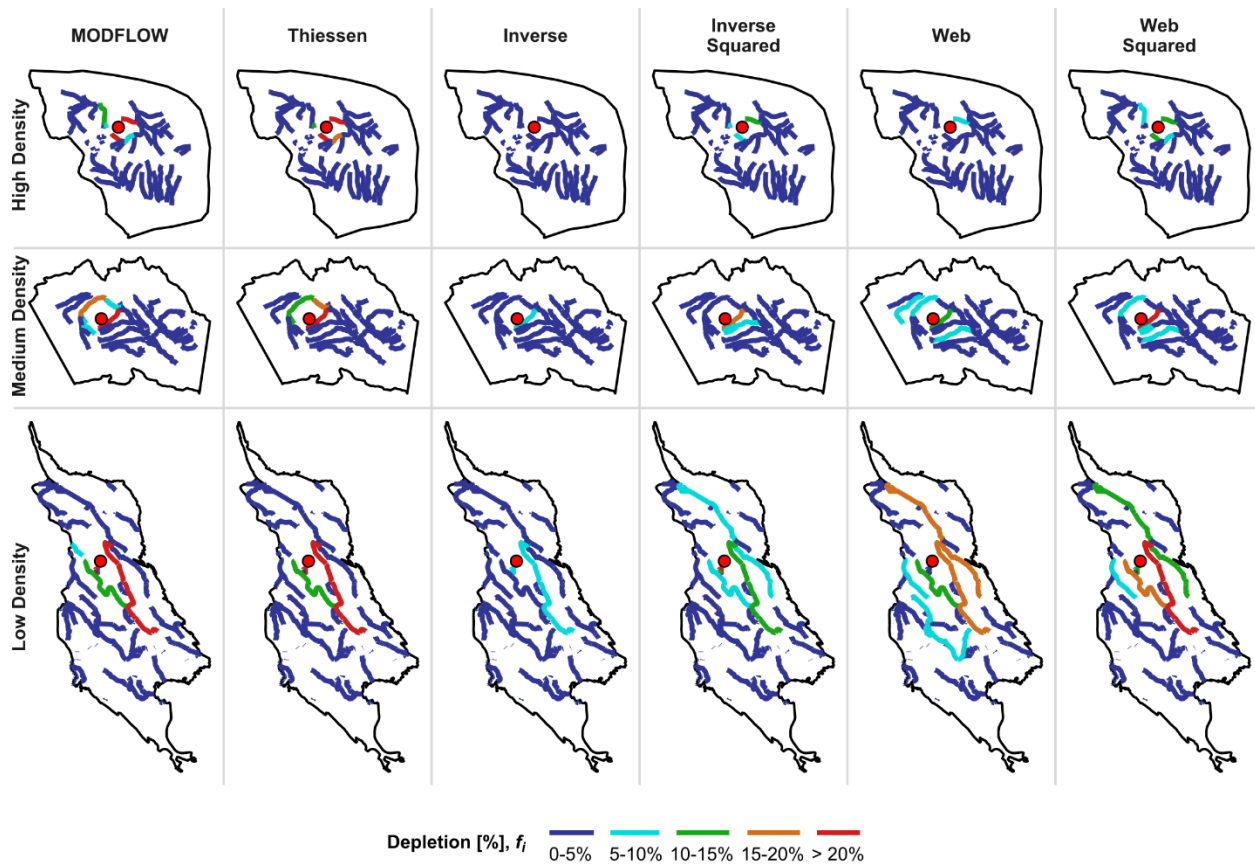
$$f_i = \frac{\Delta Q_i}{\sum_{j=1,n} \Delta Q_j} \quad \{\text{Eq. 6}\}$$

274 where ΔQ_i is the change (pumped – no pumping) in exchange between the aquifer and the cells
275 containing stream reach i . The denominator, which is the sum of ΔQ_i across all stream reaches, is
276 equal to the pumping rate (within rounding error).

277 In the flat domains, changes due to pumping were always increases in river leakage into
278 the groundwater flow system, because river cells had no exchange with the aquifer in the steady-
279 state flat case when no pumping occurred. In the simulations with topographic relief and
280 recharge, changes in river leakage could be negative in rare cases due to pumping altering the
281 local hydraulic gradient to increase flow into and through a zone containing a given stream
282 reach.

283 **2.4 Model evaluation**

284 We evaluated the performance of the different analytical apportionment equations via
285 comparison to MODFLOW output. The output variable evaluated was f_i , the fraction of total
286 streamflow depletion occurring within each stream reach for a given well, which could vary from
287 0% (the pumping well has no effect on streamflow in a given reach) to 100% (all streamflow
288 depletion from a pumping well came from a single reach). Following Reeves et al. (2009), we
289 calculated fit for a given depletion apportionment equation using only reaches with >5%
290 streamflow depletion in either the MODFLOW or depletion apportionment approaches to avoid
291 performance evaluation to be overly impacted by minor differences in small estimates of
292 depletion. As an example to illustrate the methodology, Figure 3 shows the data for an arbitrary
293 pumping well in each of the drainage density domains (corresponding to rows) with all of the
294 depletion apportionment equations (columns). For a given row, only reaches colored cyan, green,
295 orange, or red are used to compare MODFLOW and the depletion apportionment approach, and
296 dark blue reaches are ignored.



297
 298 **Figure 3.** Example plot showing estimated depletion for different stream reaches under each
 299 apportionment method for a single pumping well (red dot). Figure S1 shows a map of depletion for a
 300 given reach.

301 We used the Kling-Gupta Efficiency (KGE) as our performance metric (Gupta et al.,
 302 2009; Kling et al., 2012). The KGE decomposes error into components representing correlation,
 303 variability, and bias, thus providing more nuanced insight into model performance and the ability
 304 to weight different components of overall error compared to traditional fit metrics such as mean
 305 squared error (MSE) or Nash-Sutcliffe Efficiency (NSE; Nash & Sutcliffe, 1970). The KGE is
 306 calculated as:

$$KGE = 1 - \sqrt{S_C(r - 1)^2 + S_V(\gamma - 1)^2 + S_B(\beta - 1)^2}, \quad \{\text{Eq. 6}\}$$

$$\gamma = \frac{CV_a}{CV_n}, \quad \{\text{Eq. 7}\}$$

$$\beta = \frac{\mu_a}{\mu_n}, \quad \{\text{Eq. 8}\}$$

307 where

308 r = Pearson correlation coefficient,

309 CV = coefficient of variation of analytical (a) or numerical (n) results,

310 μ = mean of analytical (a) or numerical (n) results, and

311 S_C , S_V , and S_B = scaling factors to weight errors associated with correlation, variability,
312 and bias, respectively. For our study, these are all equal to 1 to weight error equally.

313 While the hydrologic community has traditionally used the KGE on timeseries data, our
314 model output data is spatial, corresponding to steady-state streamflow depletion estimates
315 associated with different stream reach and well combinations. This novel use for the KGE
316 allowed us to spatially evaluate both overall fit, and the performance related to correlation (r),
317 variability (γ), and bias (β). The overall KGE and each of the individual metrics (r , γ , β) have an
318 ideal value of 1.

319 To evaluate the relative contribution of correlation, variability, and bias to overall error,
320 we use the mean squared error (MSE) decomposition approach of Gupta et al. (2009) and
321 Gudmundsson et al. (2012). This approach calculates the proportion of total MSE (MSE_T) due to
322 correlation (MSE_C ; Eq. 9), variability (MSE_V ; Eq. 10), and bias (MSE_B ; Eq. 11):

$$MSE_C = \frac{2\sigma_a\sigma_n(1-r)}{MSE_T}, \quad \{\text{Eq. 9}\}$$

$$MSE_V = \frac{(\sigma_a - \sigma_n)^2}{MSE_T}, \quad \{\text{Eq. 10}\}$$

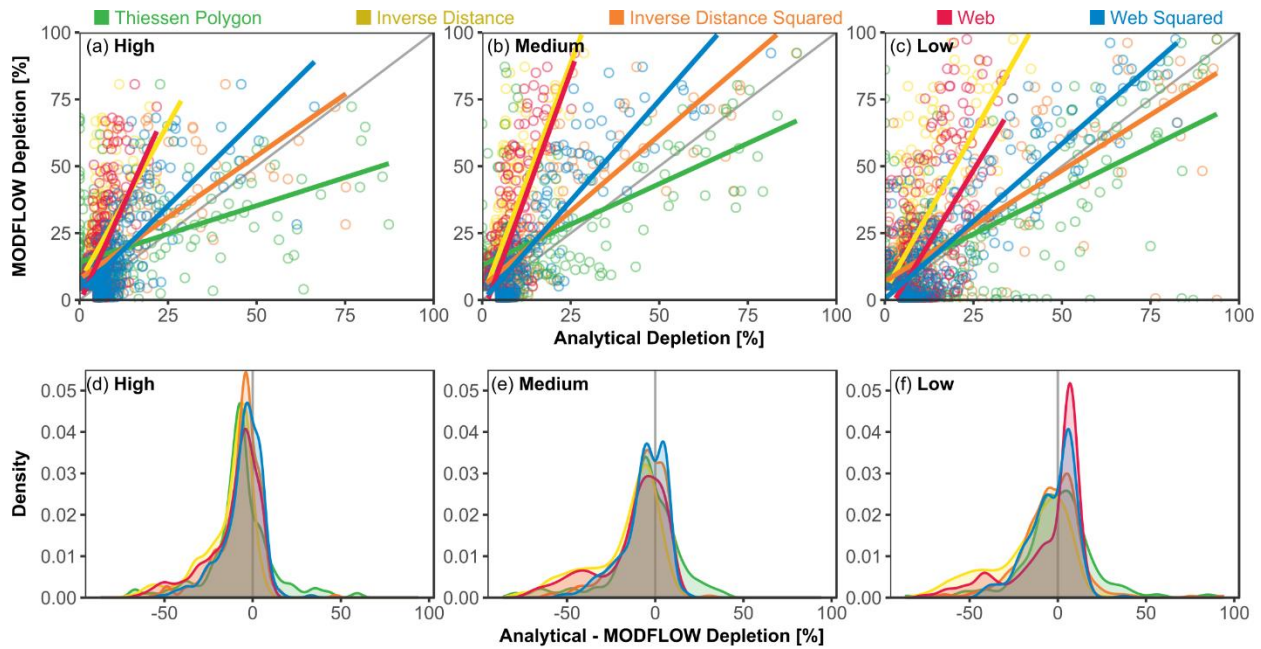
$$MSE_B = \frac{(\mu_a - \mu_n)^2}{MSE_T}, \quad \{\text{Eq. 11}\}$$

323 where σ is the population standard deviation.

324 **3 Results**

325 **3.1 Sensitivity to drainage density**

326 Across all drainage densities in the flat domains, the web squared method consistently
327 best matched MODFLOW results, followed by the inverse distance squared method (Table 3;
328 Figure 4). All depletion apportionment equations had a significant ($p < 0.001$) positive linear
329 relationships with MODFLOW estimates across all drainage densities, with R^2 values ranging
330 from 0.24 (Thiessen, low density) to 0.76 (web squared, medium density). For both the inverse
331 distance and web methods, the squared equations performed better than the linear equations
332 across all drainage densities, as the linear equations consistently underestimated depletion
333 (Figure 4a-c).



334
 335 **Figure 4.** Performance of each method and domain; only well/reach combinations with a depletion of
 336 >5% included. (a-c) MODFLOW vs. analytical depletion apportionment for high, medium, and low
 337 drainage density domains. (d-f) Difference between analytical and MODFLOW approaches for high,
 338 medium, and low drainage density domains.
 339

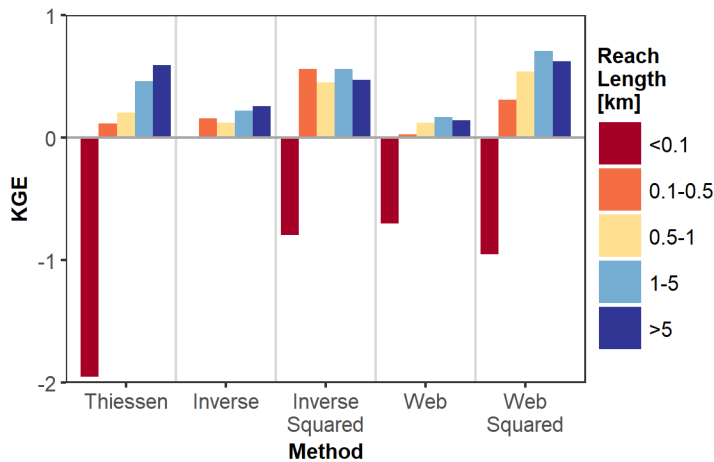
340 **Table 3.** Performance of different depletion attribution models relative to MODFLOW. Bold text is the
 341 best performance for each domain. MSE is shown in Table S1.

Drainage Density	Topography	Recharge [mm yr ⁻¹]	Kling-Gupta Efficiency (KGE)				
			Thiessen	Inverse Distance	Inverse Distance Squared	Web	Web Squared
<i>Sensitivity to drainage density in flat domains</i>							
High	No	0	-0.043	0.139	0.447	0.079	0.543
Medium	No	0	0.450	0.165	0.608	0.152	0.626
Low	No	0	0.648	0.247	0.686	0.215	0.765
<i>Sensitivity to relief and recharge in low drainage density domain</i>							
Low	Yes	0	0.573	0.169	0.590	0.100	0.596
Low	Yes	10	0.569	0.176	0.591	0.096	0.594

Low	Yes	50	0.560	0.161	0.578	0.091	0.585
Low	Yes	100	0.555	0.156	0.577	0.091	0.580
Low	Yes	500	0.520	0.130	0.545	0.065	0.535
Low	Yes	1000	0.433	0.074	0.463	0.003	0.440

342

343 For all depletion apportionment equations, performance decreased as drainage density
 344 increased, with the lowest KGE in the high density domain, intermediate in the medium density
 345 domain, and highest in the low density domain (Table 3). The decrease in performance of the
 346 depletion apportionment equations at higher drainage densities was associated with a systematic
 347 underestimation of depletion, particularly at low levels of depletion (Figure 4a,d). This pattern
 348 was strongest for the area-based Thiessen polygon method, which performed the worst in the
 349 high density domain but the third best in the medium and low density domains. However, the
 350 slope of the best fit line for the inverse distance squared and web squared approaches were
 351 closest to 1 in all domains, indicating they scale effectively across a range of depletion
 352 magnitudes in all drainage density domains.



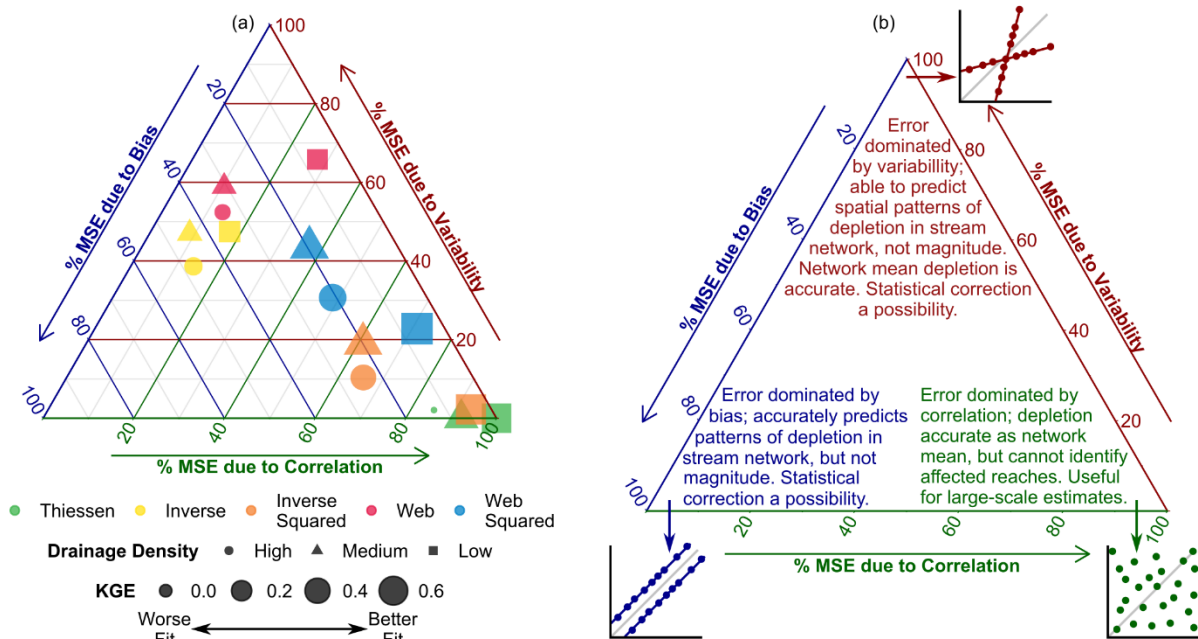
353

354 **Figure 5.** Performance of each depletion apportionment relative to MODFLOW as a function of stream
 355 reach length. See Figure S2 for distribution of stream reach lengths in each domain.

356 All of the depletion apportionment equations performed poorly at predicting depletion in
 357 short stream lengths (Figure 5), which are in many cases <0.01 km, or an order of magnitude
 358 smaller than MODFLOW cell sizes (Figure S2; Table 2). These small reaches are primarily
 359 concentrated in the low drainage density domain (Figures 2, S2, S3) at the base of a
 360 topographically steep area (Figure S4), potentially representing springs. This led to a relatively
 361 consistent spatial distribution of error across all depletion apportionment equations, though the
 362 Thiessen polygon approach also had frequent errors near the boundaries of the domain where
 363 polygons abut the domain edge in one or more directions (Figure S5). Dividing a stream into
 364 individual reaches represented by line segments is typically based on the locations of

365 confluences and short streams are a potential source of error which may be more important in
 366 highly branching stream networks.

367 The cause of error (bias, correlation, or variability) was more strongly controlled by the
 368 choice of depletion apportionment equation than drainage density (Figure 6). The web squared
 369 method, which performed the best, tended to have among the most evenly distributed error
 370 profiles with 37-71% due to correlation, 23-43% due to variability, and 6-21% due to bias. Error
 371 in the inverse distance squared method was mostly correlation (61-93%), with the remainder due
 372 to bias (5-24%) and variability (2-20%). For the Thiessen polygon approach, virtually all (85-
 373 100%) error was due to imperfect correlation. Error in the inverse distance and web methods was
 374 due primarily to variability and bias, which are linked due to the systematic underestimation of
 375 depletion by the apportionment equations (Figure 4). Across all domains and depletion
 376 apportionment equations, there was a negative bias, meaning depletion apportionment equations
 377 underpredicted depletion relative to the numerical model. This bias was negatively correlated
 378 with drainage density, with the smallest bias in the low density domain.

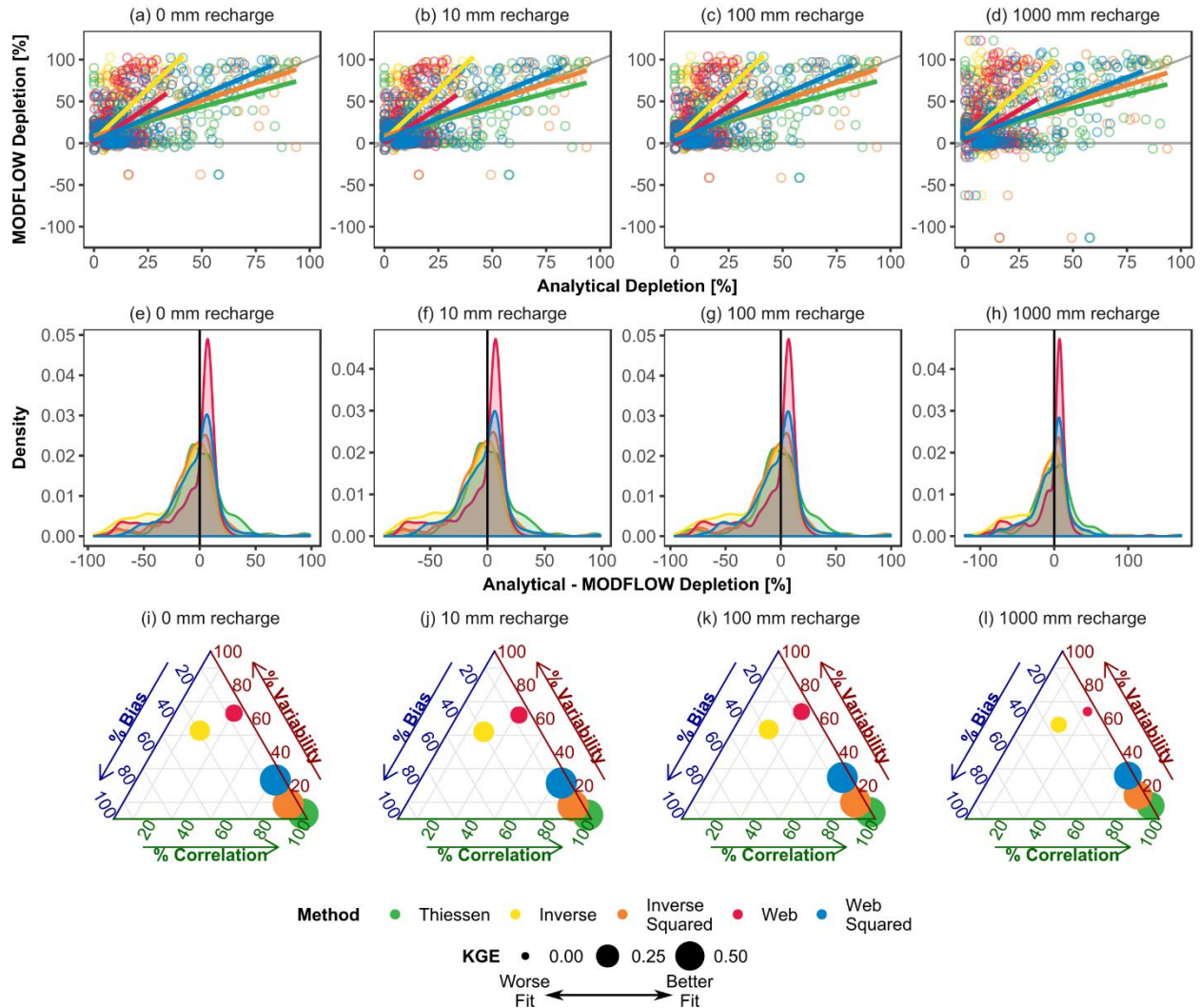


379 **Figure 6.** Ternary diagrams visualizing overall fit (KGE) and contribution of bias, variability, and
 380 correlation to total error (MSE). (a) Comparison between depletion apportionment equations and drainage
 381 density for flat, no recharge simulations. Shapes are size-coded by KGE, such that larger points have a
 382 better overall fit. (b) Annotated ternary diagram highlighting relevance of different types of error to
 383 streamflow depletion management. Pop-out scatterplots show examples analogous to Figure 4 for each
 384 endmember point of the ternary diagram.

386 3.2 Sensitivity to relief

387 When we incorporated topographic relief into the low density domain, the rank-ordering
 388 of the depletion apportionment equations remained unchanged (from best to worst: web squared,
 389 inverse distance squared, Thiessen polygon, inverse distance, web; Table 3), though the gap
 390 between the web squared and inverse distance squared methods decreases dramatically. For the
 391 best method, web squared, the decrease in performance due to the introduction of relief into the

392 low density domain was approximately equal to the decrease in performance associated with
 393 going from low to medium drainage density (Table 3). However, while performance skill
 394 decreased due to relief, the patterns of performance were comparable with the flat domain; for
 395 example, the inverse distance squared method had the closest slope to 1.0 (Figure 7a), the inverse
 396 distance and web methods consistently underestimated depletion (Figure 7a,e), and the causes of
 397 variability remained primarily correlation errors for the best-performing approaches (Figure 7i),
 398 especially Thiessen polygon. As in the flat domains, there was a negative bias for all depletion
 399 apportionment equations, with the smallest bias using the Thiessen polygon approach.



400
 401 **Figure 7.** Sensitivity to topographic relief and recharge for each domain. Top two rows are analogous to
 402 Figure 4, and bottom row to Figure 6. Recharge rates are shown next to figure letters.

403 3.3 Sensitivity to recharge

404 As the amount of groundwater recharge increased, the performance of all depletion
 405 apportionment equations decreased (Table 3). Web squared performed the best at recharge rates
 406 $\leq 100 \text{ mm yr}^{-1}$ (followed by inverse distance squared), while inverse distance squared performed
 407 the best at recharge rates $\geq 500 \text{ mm yr}^{-1}$ (followed by web squared). Despite this change in rank

408 order at high recharge levels, the performance of the web squared and inverse distance squared
409 were extremely similar across all recharge rates, differing only at the second decimal place of
410 KGE for recharge rates $\leq 1000 \text{ mm yr}^{-1}$, and MSE for the web squared method was lowest for all
411 scenarios simulated (Table 3, Table S1). As noted with the introduction of relief (Section 3.2),
412 the patterns of performance remained comparable both to the flat domain and among different
413 recharge rates: the slope of the inverse distance squared was closest to 1.0 (Figure 7a-d),
414 depletion was consistently underestimated by the inverse distance and web methods (Figure 7a-
415 h), and the causes of error for the best-performing approaches remained correlation errors for the
416 best-performing approaches (Figure 7i-l), especially Thiessen polygon.

417 For several well-reach combinations, MODFLOW-predicted depletion was either $<0\%$
418 (meaning less river leakage when the well was pumped) or $>100\%$ (meaning greater than the
419 total leakage summed across all reaches). These two unusual circumstances are by definition
420 related in Eq. 6: it is impossible for depletion of $>100\%$ to occur in a reach without negative
421 depletion occurring elsewhere in the domain. Negative depletion estimates occurred when high
422 recharge rates led to strong head gradients, including head rising above the surface elevation
423 (Figure S4), due to the no-flow boundaries along the edges of our no-flow domain. Pumping
424 slightly reduced the gradients in places, leading to changes in watershed divide locations.

425 **4 Discussion**

426 **4.1 Depletion apportionment equation performance**

427 In order to use analytical streamflow depletion models as effective groundwater-surface
428 water management tools, it is necessary to understand where and under what conditions they
429 perform effectively. Previous work by Reeves et al. (2009) tested nine depletion apportionment
430 equations for a single stream reach in Michigan, and concluded that an inverse distance
431 weighting approach using the closest point on each stream reach to a well was reasonably
432 effective in comparison with numerical model results and grounded in hydrogeologic theory
433 (Wilson, 1993). In this study, we tested this conclusion in a variety of settings including multiple
434 stream network geometries, topography, and groundwater recharge conditions. We found that a
435 new method introduced here (web squared) outperforms the inverse distance approach under
436 most of the conditions simulated (Table 3; Table S1). This indicates that complete stream
437 network geometry, rather than a single point on each stream, is a critical consideration for the
438 accurate use of analytical solutions.

439 Stream length was an important control on the performance of all of the depletion
440 apportionment equations, with a substantially worse fit to MODFLOW results in very short (<0.1
441 km) stream reaches (Figure 5). These short streams are found primarily in the low density
442 domain at the base of a topographically-steep feature and potentially represent springs, a type of
443 groundwater-dependent ecosystem which is particularly vulnerable to pumping (Currell, 2016;
444 Eamus et al., 2015; Rohde et al., 2017). Given that the length of these reaches is smaller than the
445 MODFLOW grid cells used to represent them, this error may be driven by a scale mismatch
446 between the two methods; finer meshes in numerical models may be necessary to accurately
447 estimate depletion in these short reaches.

448 **4.2 Importance of different sources of error**

449 In this study, we apply the KGE spatially and develop a novel approach to quantifying
450 and visualizing the contribution of different sources of error (e.g. Figure 6). We weighted the
451 different types of error (correlation, bias, variability) equally in the calculation of the KGE.
452 However, depending on study, policy or management goals it is possible to assign different
453 weights to these components which may influence the selection of the preferred depletion
454 apportionment equation. Figure 6b highlights some of the considerations associated with
455 different types of error. For instance, methods where error is primarily due to bias and variability
456 are best at identifying which streams are affected by a pumping well, though the magnitude of
457 depletion may be incorrect – though this may be statistically corrected if the degree of
458 bias/variability is known. In contrast, methods where the error is primarily due to correlation are
459 most effective at predicting mean network-wide depletion, but not identifying specific reaches
460 which may be affected. Given that the error in the web squared method tends to be less
461 associated with correlation than either the inverse distance squared or Thiessen polygon
462 approaches, this is further support for its use in screening for potential streamflow depletion.

463 The prioritization of different types of errors, therefore, is a local decision depending on
464 social and political priorities (Acreman et al., 2014; Quevauviller et al., 2016). The flexibility of
465 the KGE and the ability to decompose mean squared error into its various components
466 (Gudmundsson et al., 2012; Gupta et al., 2009) makes it a valuable tool for assessing depletion
467 apportionment equations. For environmental reasons, conservative estimates of depletion are
468 preferred as they avoid overallocation of water resources (Gleeson & Richter, 2017; Jayawan et
469 al., 2016; Rathfelder, 2016; Reeves et al., 2009). Concerningly, all of the depletion
470 apportionment equations tested here had a negative bias in our archetypal domain, ranging from -
471 0.2% (Thiessen polygon, flat low density domain) to -72.2% (inverse distance, flat high density
472 domain) (Figures 4, 7). A negative bias means that (on average) streamflow depletion will be
473 underestimated when using the depletion apportionment equation relative to the numerical
474 model. This differs from previous work by Rathfelder (2016), which found that analytical
475 models tended to overpredict depletion relative to a calibrated numerical model; however,
476 Rathfelder (2016) was looking at transient depletion for a single stream over a relatively short (2
477 year) timeframe, while our study investigates long-term steady-state depletion distributed among
478 a network. These results highlight the importance of quantifying bias locally and correcting
479 where possible.

480 **4.3 Future research needs**

481 We also note several factors impacting streamflow depletion raised by this study which
482 will be explored in future work. First, model boundary conditions should be sufficiently far from
483 both the wells and the stream reaches of interest. Where non-flowing surface water features such
484 as a coastline are present, these can introduce a considerable source of error, as depletion
485 apportionment equations have not been tested for variable density flow (e.g. saltwater intrusion).
486 Second, given that streams may potentially dry as a result of pumping which can lead to
487 nonlinearities in the baseflow response to pumping (Ahlfeld et al., 2016), the streamflow-routing
488 (SFR; Niswonger & Prudic, 2005) MODFLOW package may be preferred to the river (RIV)
489 package used in this study (Feinstein et al., 2016; Fienen et al., 2018). However, given that

490 analytical models typically assume that streams will not dry, using SFR would be less directly
491 comparable to analytical model results. Finally, as noted in Section 2, this study focused on the
492 effects of stream geometry, and we do not assess the sensitivity of our results to subsurface
493 parameters controlling groundwater flow such as hydraulic conductivity and streambed
494 conductance.

495 **5 Synthesis and conclusions**

496 Groundwater is widely used for irrigation around the world and groundwater pumping
497 can be a major driver to low streamflow, particularly by exacerbating hydrologic drought (de
498 Graaf et al., 2014; Siebert et al., 2010; Veldkamp et al., 2017; Wada et al., 2012, 2013). To avoid
499 negative impacts of streamflow depletion on ecosystems and stakeholders, it is essential to both
500 quantify the source of water used by wells and put that knowledge into the hands of management
501 decision-makers (Gleeson et al., 2012; Irvine, 2018; Van Loon et al., 2016). Due to the high
502 effort, expertise, and data required to make a site-specific numerical model (Table 1), analytical
503 models paired with depletion apportionment equations may be an essential management tool that
504 can be used to screen pumping wells to avoid excessive depletion.

505 This study makes a major advance towards the development of such tools by evaluating
506 the performance of a suite of depletion apportionment equations across a range of stream
507 network geometries. From this, we conclude:

- 508 (1) Web-squared, a new method introduced here which explicitly considers stream network
509 geometry, performs the best across a range of drainage density, topographic, and
510 groundwater recharge scenarios, followed by the inverse distance squared method.
- 511 (2) The performance of all depletion apportionment equations decreases as drainage density
512 increased, topographic relief was included, groundwater recharge increased, and stream
513 reach length shortened.
- 514 (3) The KGE and error decomposition approaches demonstrated here are valuable metrics for
515 assessing the performance of streamflow depletion approaches, as it allows for the
516 separate assessment of performance criteria (correlation, bias, variability) with different
517 management implications.

518 Future work is needed to test the performance of these depletion attribution methods in different
519 hydrostratigraphic settings, and including additional complexity such as subsurface heterogeneity
520 and transient groundwater flow conditions, to better constrain their use as conjunctive
521 groundwater-surface water management tools.

522 **6 Acknowledgments**

523 We appreciate helpful discussions with Ben Kerr and Tara Forstner during the analysis and
524 writing process. This work was funded by a Natural Sciences and Engineering Research Council
525 Collaborative Research and Development Grant (NSERC CRD) to the University of Victoria and
526 Foundry Spatial. Support to Andreas Hartmann was provided by the Emmy Noether-Programme
527 of the German Research Foundation (DFG; grant number HA 8113/1-1; project ‘Global

528 Assessment of Water Stress in Karst Regions in a Changing World'). Data and analysis scripts
529 are available on GitHub (<https://github.com/szipper/NanaimoAttributionMethods>). All analyses
530 were performed using R 3.4.3 (R Core Team, 2017) and graphics were made using ggplot2
531 (Wickham, 2009), ggtern (Hamilton, 2017), and InkScape (The Inkscape Team, 2015).

532 7 References

- 533 Acreman, M. C., Overton, I. C., King, J., Wood, P. J., Cowx, I. G., Dunbar, M. J., ... Young, W. J.
534 (2014). The changing role of ecohydrological science in guiding environmental flows.
535 *Hydrological Sciences Journal*, 59(3–4), 433–450.
536 <https://doi.org/10.1080/02626667.2014.886019>
- 537 Ahlfeld, D. P., Schneider, J. C., & Spalding, C. P. (2016). Effects of nonlinear model response on
538 allocation of streamflow depletion: exemplified by the case of Beaver Creek, USA. *Hydrogeology*
539 *Journal*, 24(7), 1835–1845. <https://doi.org/10.1007/s10040-016-1438-3>
- 540 Barlow, P. M., & Leake, S. A. (2012). *Streamflow depletion by wells--Understanding and managing the*
541 *effects of groundwater pumping on streamflow* (No. Circular 1376). Reston VA: U.S. Geological
542 Survey.
- 543 Booth, E. G., Zipper, S. C., Loheide, S. P., & Kucharik, C. J. (2016). Is groundwater recharge always
544 serving us well? Water supply provisioning, crop production, and flood attenuation in conflict in
545 Wisconsin, USA. *Ecosystem Services*, 21, Part A, 153–165.
546 <https://doi.org/10.1016/j.ecoser.2016.08.007>
- 547 Bredehoeft, J. D. (2002). The Water Budget Myth Revisited: Why Hydrogeologists Model. *Ground*
548 *Water*, 40(4), 340–345. <https://doi.org/10.1111/j.1745-6584.2002.tb02511.x>
- 549 Bredehoeft, J. D., Papadopulos, S. S., & Cooper, H. H. (1982). Groundwater: The water budget myth.
550 *Scientific Basis of Water Resource Management*, 51, 57.
- 551 Bredehoeft, J., & Kendy, E. (2008). Strategies for Offsetting Seasonal Impacts of Pumping on a Nearby
552 Stream. *Ground Water*, 46(1), 23–29. <https://doi.org/10.1111/j.1745-6584.2007.00367.x>
- 553 Butler, J. J., Zlotnik, V. A., & Tsou, M.-S. (2001). Drawdown and Stream Depletion Produced by
554 Pumping in the Vicinity of a Partially Penetrating Stream. *Ground Water*, 39(5), 651–659.
555 <https://doi.org/10.1111/j.1745-6584.2001.tb02354.x>
- 556 Currell, M. J. (2016). Drawdown “Triggers”: A Misguided Strategy for Protecting Groundwater-Fed
557 Streams and Springs. *Groundwater*, 54(5), 619–622. <https://doi.org/10.1111/gwat.12425>
- 558 Eamus, D., Zolfaghar, S., Villalobos-Vega, R., Cleverly, J., & Huete, A. (2015). Groundwater-dependent
559 ecosystems: recent insights from satellite and field-based studies. *Hydrology and Earth System*
560 *Sciences*, 19(10), 4229–4256. <https://doi.org/10.5194/hess-19-4229-2015>
- 561 Feinstein, D. T., Fienen, M. N., Reeves, H. W., & Langevin, C. D. (2016). A Semi-Structured
562 MODFLOW-USG Model to Evaluate Local Water Sources to Wells for Decision Support.
563 *Groundwater*, 54(4), 532–544. <https://doi.org/10.1111/gwat.12389>
- 564 Fetter, C. W. (2000). *Applied Hydrogeology* (4 edition). Upper Saddle River, N.J: Pearson.
- 565 Fienen, M. N., Bradbury, K. R., Kniffin, M., & Barlow, P. M. (2018). Depletion Mapping and
566 Constrained Optimization to Support Managing Groundwater Extraction. *Groundwater*, 56(1),
567 18–31. <https://doi.org/10.1111/gwat.12536>
- 568 Foglia, L., McNally, A., & Harter, T. (2013). Coupling a spatiotemporally distributed soil water budget
569 with stream-depletion functions to inform stakeholder-driven management of groundwater-
570 dependent ecosystems. *Water Resources Research*, 49(11), 7292–7310.
571 <https://doi.org/10.1002/wrcr.20555>
- 572 Gleeson, T., Befus, K. M., Jasechko, S., Luijendijk, E., & Cardenas, M. B. (2016). The global volume and
573 distribution of modern groundwater. *Nature Geoscience*, 9(2), 161–167.
574 <https://doi.org/10.1038/ngeo2590>

- 575 Gleeson, T., & Richter, B. (2017). How much groundwater can we pump and protect environmental flows
576 through time? Presumptive standards for conjunctive management of aquifers and rivers. *River*
577 *Research and Applications*. <https://doi.org/10.1002/rra.3185>
- 578 Gleeson, T., Alley, W. M., Allen, D. M., Sophocleous, M. A., Zhou, Y., Taniguchi, M., & VanderSteen,
579 J. (2012). Towards sustainable groundwater use: Setting long-term goals, backcasting, and
580 managing adaptively. *Ground Water*, 50(1), 19–26. <https://doi.org/10.1111/j.1745->
581 6584.2011.00825.x
- 582 Glover, R. E., & Balmer, G. G. (1954). River depletion resulting from pumping a well near a river. *Eos,*
583 *Transactions American Geophysical Union*, 35(3), 468–470.
584 <https://doi.org/10.1029/TR035i003p00468>
- 585 Government of Canada. (2016, January 25). National Hydro Network. Retrieved January 16, 2018, from
586 <http://open.canada.ca/data/en/dataset/a4b190fe-e090-4e6d-881e-b87956c07977>
- 587 de Graaf, I. E. M., van Beek, L. P. H., Wada, Y., & Bierkens, M. F. P. (2014). Dynamic attribution of
588 global water demand to surface water and groundwater resources: Effects of abstractions and
589 return flows on river discharges. *Advances in Water Resources*, 64, 21–33.
590 <https://doi.org/10.1016/j.advwatres.2013.12.002>
- 591 Gudmundsson, L., Wagener, T., Tallaksen, L. M., & Engeland, K. (2012). Evaluation of nine large-scale
592 hydrological models with respect to the seasonal runoff climatology in Europe. *Water Resources*
593 *Research*, 48(11), W11504. <https://doi.org/10.1029/2011WR010911>
- 594 Gupta, H. V., Kling, H., Yilmaz, K. K., & Martinez, G. F. (2009). Decomposition of the mean squared
595 error and NSE performance criteria: Implications for improving hydrological modelling. *Journal*
596 *of Hydrology*, 377(1), 80–91. <https://doi.org/10.1016/j.jhydrol.2009.08.003>
- 597 Hamilton, N. (2017). ggtern: An Extension to “ggplot2”, for the Creation of Ternary Diagrams (Version
598 2.2.1). Retrieved from <https://CRAN.R-project.org/package=ggtern>
- 599 Hantush, M. S. (1965). Wells near streams with semipervious beds. *Journal of Geophysical Research*,
600 70(12), 2829–2838. <https://doi.org/10.1029/JZ070i012p02829>
- 601 Harbaugh, A. W. (2005). *MODFLOW-2005: the U.S. Geological Survey modular ground-water model--*
602 *the ground-water flow process* (USGS Numbered Series No. 6-A16). U.S. Geological Survey.
603 Retrieved from <http://pubs.er.usgs.gov/publication/tm6A16>
- 604 Hunt, B. (1999). Unsteady Stream Depletion from Ground Water Pumping. *Ground Water*, 37(1), 98–
605 102. <https://doi.org/10.1111/j.1745-6584.1999.tb00962.x>
- 606 Irvine, D. J. (2018). Bridging the Gap Between Research and Practice. *Groundwater*, 56(1), 1–1.
607 <https://doi.org/10.1111/gwat.12616>
- 608 Jayawan, I. S., Demond, A. H., & Ellis, B. R. (2016). Emerging investigators series: using an analytical
609 solution approach to permit high volume groundwater withdrawals. *Environmental Science:*
610 *Water Research & Technology*, 2(6), 942–952. <https://doi.org/10.1039/C6EW00108D>
- 611 Jenkins, C. T. (1968). Techniques for Computing Rate and Volume of Stream Depletion by Wells.
612 *Ground Water*, 6(2), 37–46. <https://doi.org/10.1111/j.1745-6584.1968.tb01641.x>
- 613 Johnson, Z. C., Snyder, C. D., & Hitt, N. P. (2017). Landform features and seasonal precipitation predict
614 shallow groundwater influence on temperature in headwater streams. *Water Resources Research*,
615 53(7), 5788–5812. <https://doi.org/10.1002/2017WR020455>
- 616 Kendy, E., & Bredehoeft, J. D. (2006). Transient effects of groundwater pumping and surface-water-
617 irrigation returns on streamflow. *Water Resources Research*, 42(8), W08415.
618 <https://doi.org/10.1029/2005WR004792>
- 619 Kling, H., Fuchs, M., & Paulin, M. (2012). Runoff conditions in the upper Danube basin under an
620 ensemble of climate change scenarios. *Journal of Hydrology*, 424–425(Supplement C), 264–277.
621 <https://doi.org/10.1016/j.jhydrol.2012.01.011>
- 622 Konikow, L. F., & Leake, S. A. (2014). Depletion and Capture: Revisiting “The Source of Water Derived
623 from Wells”.” *Groundwater*, 52, 100–111. <https://doi.org/10.1111/gwat.12204>
- 624 Kurylyk, B. L., MacQuarrie, K. T. B., & McKenzie, J. M. (2014). Climate change impacts on
625 groundwater and soil temperatures in cold and temperate regions: Implications, mathematical

theory, and emerging simulation tools. *Earth-Science Reviews*, 138, 313–334.
<https://doi.org/10.1016/j.earscirev.2014.06.006>

628 Kurylyk, B. L., MacQuarrie, K. T. B., Caissie, D., & McKenzie, J. M. (2015). Shallow groundwater
629 thermal sensitivity to climate change and land cover disturbances: derivation of analytical
630 expressions and implications for stream temperature modeling. *Hydrology and Earth System
631 Sciences*, 19(5), 2469–2489. <https://doi.org/10.5194/hess-19-2469-2015>

632 Lackey, G., Neupauer, R. M., & Pitlick, J. (2015). Effects of Streambed Conductance on Stream
633 Depletion. *Water*, 7(1), 271–287. <https://doi.org/10.3390/w7010271>

634 Leake, S. A., Reeves, H. W., & Dickinson, J. E. (2010). A New Capture Fraction Method to Map How
635 Pumpage Affects Surface Water Flow. *Ground Water*, 48(5), 690–700.
636 <https://doi.org/10.1111/j.1745-6584.2010.00701.x>

637 Li, B.-D., Sampath, P. V., & Liao, H. (2016). A study on the hydro-geologic factors that affect
638 streamflow depletion. *Hydrological Sciences Journal*, 61(11), 2133–2143.
639 <https://doi.org/10.1080/02626667.2015.1083649>

640 Miller, C. D., Durnford, D., Halstead, M. R., Altenhofen, J., & Flory, V. (2007). Stream Depletion in
641 Alluvial Valleys Using the SDF Semianalytical Model. *Ground Water*, 45(4), 506–514.
642 <https://doi.org/10.1111/j.1745-6584.2007.00311.x>

643 Nash, J. E., & Sutcliffe, J. V. (1970). River flow forecasting through conceptual models part I — A
644 discussion of principles. *Journal of Hydrology*, 10(3), 282–290. [https://doi.org/10.1016/0022-1694\(70\)90255-6](https://doi.org/10.1016/0022-1694(70)90255-6)

645 Natural Resources Canada. (1997). *Canada Digital Elevation Data*. Ottawa, ON.

646 Niswonger, R. G., & Prudic, D. E. (2005). *Documentation of the Streamflow-Routing (SFR2) Package to
647 Include Unsaturated Flow Beneath Streams - A Modification to SFR1* (USGS Numbered Series
648 No. 6-A13) (p. 57). U.S. Geological Survey. Retrieved from
649 <http://pubs.er.usgs.gov/publication/tm6A13>

650 Nyholm, T., Christensen, S., & Rasmussen, K. R. (2002). Flow Depletion in a Small Stream Caused by
651 Ground Water Abstraction from Wells. *Ground Water*, 40(4), 425–437.
652 <https://doi.org/10.1111/j.1745-6584.2002.tb02521.x>

653 Quevauviller, P., Batelaan, O., & Hunt, R. J. (2016). Groundwater Regulation and Integrated Water
654 Planning. In *Integrated Groundwater Management* (pp. 197–227). Springer, Cham.
655 https://doi.org/10.1007/978-3-319-23576-9_8

656 R Core Team. (2017). R: A language and environment for statistical computing (Version 3.4.3). Vienna,
657 Austria: R Foundation for Statistical Computing. Retrieved from <https://www.R-project.org/>

658 Rathfelder, K. M. (2016). *Modelling tools for estimating effects of groundwater pumping on surface
659 waters* (Water Science Series No. WSS2016-09). Province of B.C.: Ministry of Environment.

660 Reeves, H. W., Hamilton, D. A., Seelbach, P. W., & Asher, A. J. (2009). *Ground-water-withdrawal
661 component of the Michigan water-withdrawal screening tool* (Scientific Investigations Report
662 No. 2009–5003) (p. 36). Reston VA: U.S. Geological Survey. Retrieved from
663 <https://pubs.usgs.gov/sir/2009/5003/>

664 Rohde, M. M., Froend, R., & Howard, J. (2017). A Global Synthesis of Managing Groundwater
665 Dependent Ecosystems Under Sustainable Groundwater Policy. *Groundwater*, n/a-n/a.
666 <https://doi.org/10.1111/gwat.12511>

667 Siebert, S., Burke, J., Faures, J. M., Frenken, K., Hoogeveen, J., Doell, P., & Portmann, F. T. (2010).
668 Groundwater use for irrigation - a global inventory. *Hydrology and Earth System Sciences*,
669 14(10), 1863–1880. <https://doi.org/10.5194/hess-14-1863-2010>

670 Sophocleous, M., Koussis, A., Martin, J. L., & Perkins, S. P. (1995). Evaluation of Simplified Stream-
671 Aquifer Depletion Models for Water Rights Administration. *Ground Water*, 33(4), 579–588.
672 <https://doi.org/10.1111/j.1745-6584.1995.tb00313.x>

673 Spalding, C. P., & Khaleel, R. (1991). An evaluation of analytical solutions to estimate drawdowns and
674 stream depletions by wells. *Water Resources Research*, 27(4), 597–609.
675 <https://doi.org/10.1029/91WR00001>

676

677 Strauch, A. M., MacKenzie, R. A., & Tingley, R. W. (2017). Base flow-driven shifts in tropical stream
678 temperature regimes across a mean annual rainfall gradient. *Hydrological Processes*, 31(9),
679 1678–1689. <https://doi.org/10.1002/hyp.11084>

680 The Inkscape Team. (2015). Inkscape (Version 0.91). Retrieved from <https://inkscape.org/en/>

681 Theis, C. V. (1941). The effect of a well on the flow of a nearby stream. *Eos, Transactions American*
682 *Geophysical Union*, 22(3), 734–738. <https://doi.org/10.1029/TR022i003p00734>

683 Van Loon, A. F., Gleeson, T., Clark, J., Van Dijk, A. I. J. M., Stahl, K., Hannaford, J., ... Van Lanen, H.
684 A. J. (2016). Drought in the Anthropocene. *Nature Geoscience*, 9(2), 89–91.
685 <https://doi.org/10.1038/ngeo2646>

686 Veldkamp, T. I. E., Wada, Y., Aerts, J. C. J. H., Döll, P., Gosling, S. N., Liu, J., ... Ward, P. J. (2017).
687 Water scarcity hotspots travel downstream due to human interventions in the 20th and 21st
688 century. *Nature Communications*, 8, ncomms15697. <https://doi.org/10.1038/ncomms15697>

689 Voss, C. I. (2011a). Editor’s message: Groundwater modeling fantasies —part 1, adrift in the details.
690 *Hydrogeology Journal*, 19(7), 1281–1284. <https://doi.org/10.1007/s10040-011-0789-z>

691 Voss, C. I. (2011b). Editor’s message: Groundwater modeling fantasies—part 2, down to earth.
692 *Hydrogeology Journal*, 19(8), 1455–1458. <https://doi.org/10.1007/s10040-011-0790-6>

693 Wada, Y., van Beek, L. P. H., & Bierkens, M. F. P. (2012). Nonsustainable groundwater sustaining
694 irrigation: A global assessment. *Water Resources Research*, 48(6), W00L06.
695 <https://doi.org/10.1029/2011WR010562>

696 Wada, Y., van Beek, L. P. H., Wanders, N., & Bierkens, M. F. P. (2013). Human water consumption
697 intensifies hydrological drought worldwide. *Environmental Research Letters*, 8(3), 034036.
698 <https://doi.org/10.1088/1748-9326/8/3/034036>

699 Wickham, H. (2009). *ggplot2: Elegant Graphics for Data Analysis*. Springer-Verlag New York.
700 Retrieved from <http://ggplot2.org>

701 Wilson, J. L. (1993). Induced infiltration in aquifers with ambient flow. *Water Resources Research*,
702 29(10), 3503–3512. <https://doi.org/10.1029/93WR01393>

703 Zektser, S., Loáiciga, H. A., & Wolf, J. T. (2005). Environmental impacts of groundwater overdraft:
704 selected case studies in the southwestern United States. *Environmental Geology*, 47(3), 396–404.
705 <https://doi.org/10.1007/s00254-004-1164-3>

706 Zipper, S. C., Soyulu, M. E., Kucharik, C. J., & Loheide II, S. P. (2017). Quantifying indirect groundwater-
707 mediated effects of urbanization on agroecosystem productivity using MODFLOW-AgroIBIS
708 (MAGI), a complete critical zone model. *Ecological Modelling*, 359, 201–219.
709 <https://doi.org/10.1016/j.ecolmodel.2017.06.002>

710 Zorn, T. G., Seelbach, P. W., & Rutherford, E. S. (2012). A Regional-Scale Habitat Suitability Model to
711 Assess the Effects of Flow Reduction on Fish Assemblages in Michigan Streams. *JAWRA*
712 *Journal of the American Water Resources Association*, 48(5), 871–895.
713 <https://doi.org/10.1111/j.1752-1688.2012.00656.x>

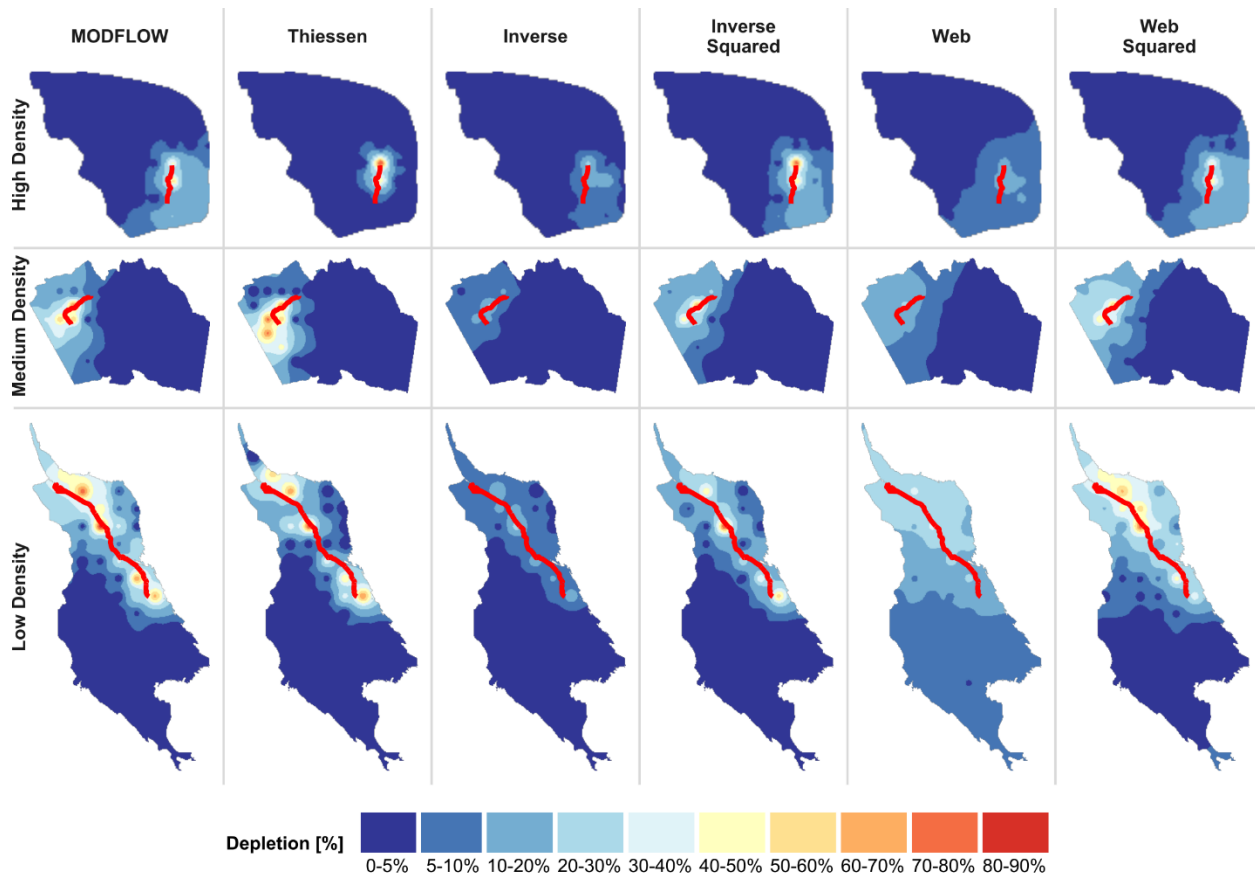
714

715 **8 Supplemental Tables and Figures**

716 **Table S1.** Mean squared error of different depletion attribution models relative to MODFLOW. Bold text
 717 is the best performance for each domain.

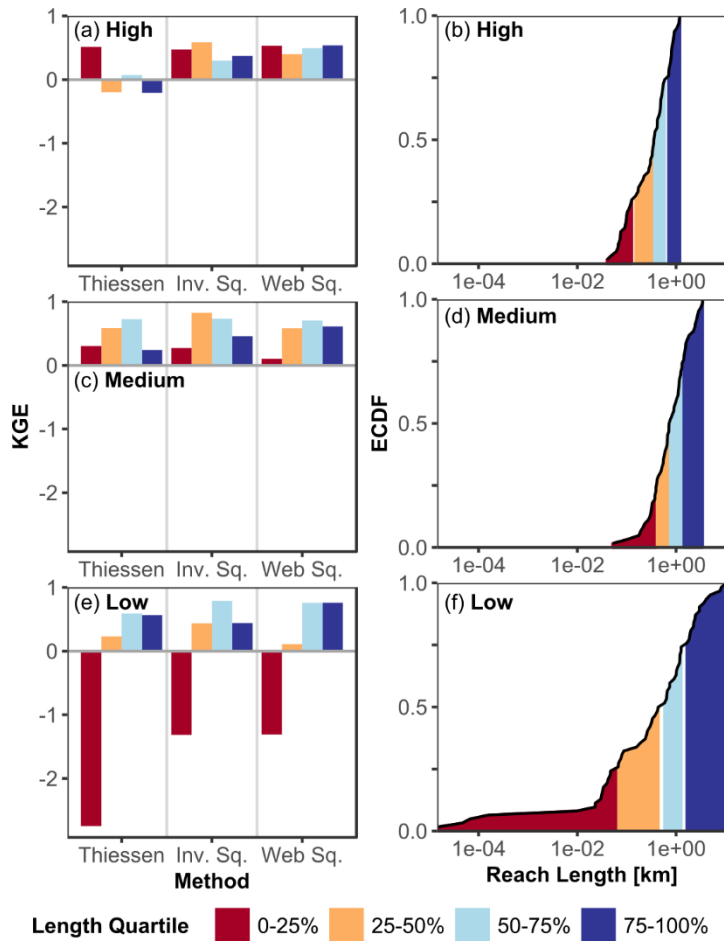
Drainage Density	Topography	Recharge [mm yr ⁻¹]	Mean Squared Error (MSE) [% Points]				
			Thiessen	Inverse Distance	Inverse Distance Squared	Web	Web Squared
<i>Sensitivity to drainage density in flat domains</i>							
High	No	0	385.4	418.8	204.8	350.3	167.0
Medium	No	0	420.2	672.2	227.6	532.2	189.9
Low	No	0	442.5	693.2	309.6	420.2	172.3
<i>Sensitivity to relief and recharge in low drainage density domain</i>							
Low	Yes	0	627.2	943.0	521.0	604.2	426.6
Low	Yes	10	620.4	907.3	503.1	589.2	421.9
Low	Yes	50	651.2	960.4	545.6	617.4	445.3
Low	Yes	100	671.4	997.3	562.4	632.9	460.7
Low	Yes	500	755.5	1078.4	645.3	690.5	546.8
Low	Yes	1000	969.2	1274.9	853.9	800.2	735.2

718



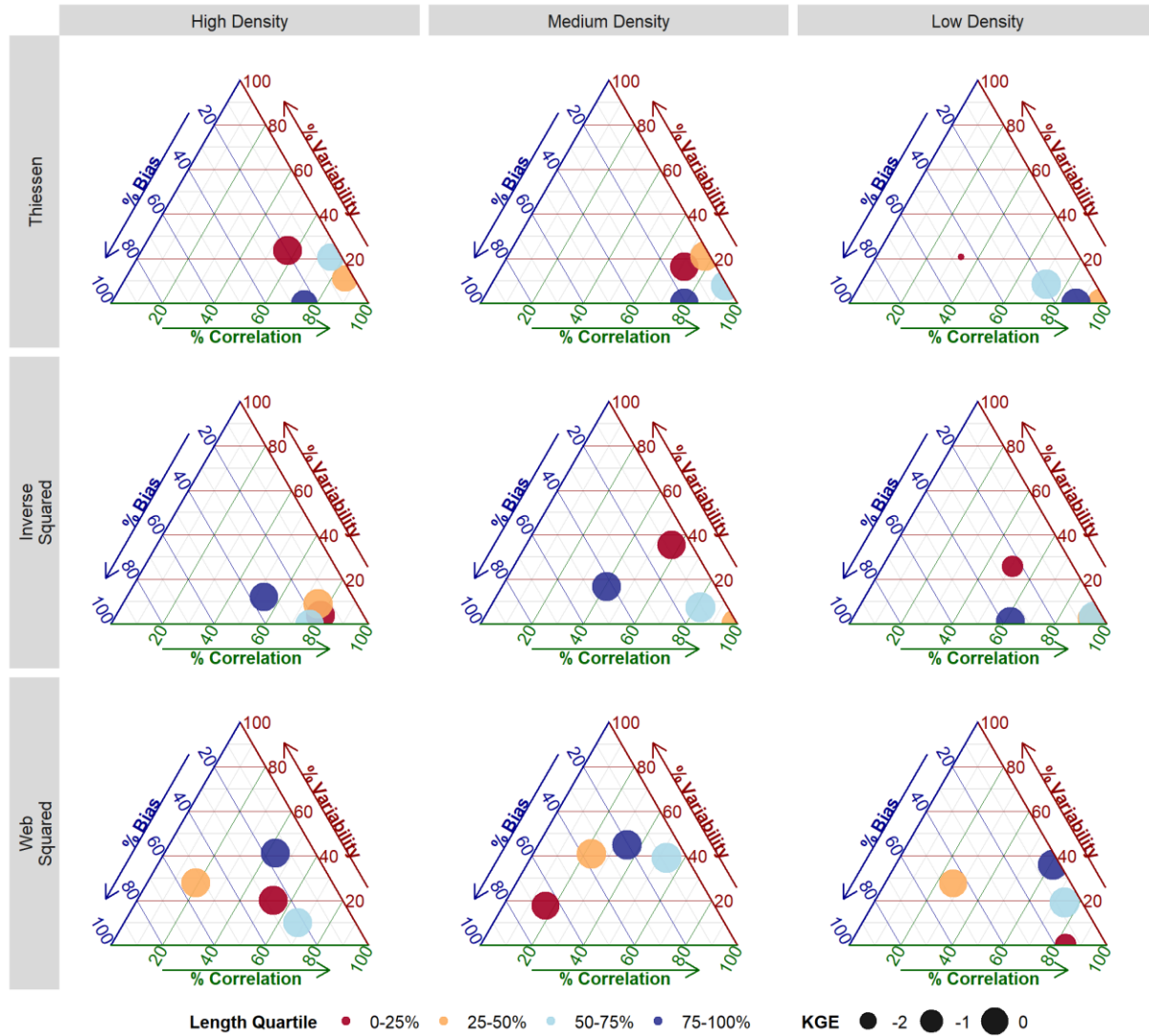
719
 720
 721
 722

Figure S1. Estimated depletion for a given stream reach as a function of pumping well location, interpolated from each well using inverse distance weighted kriging.



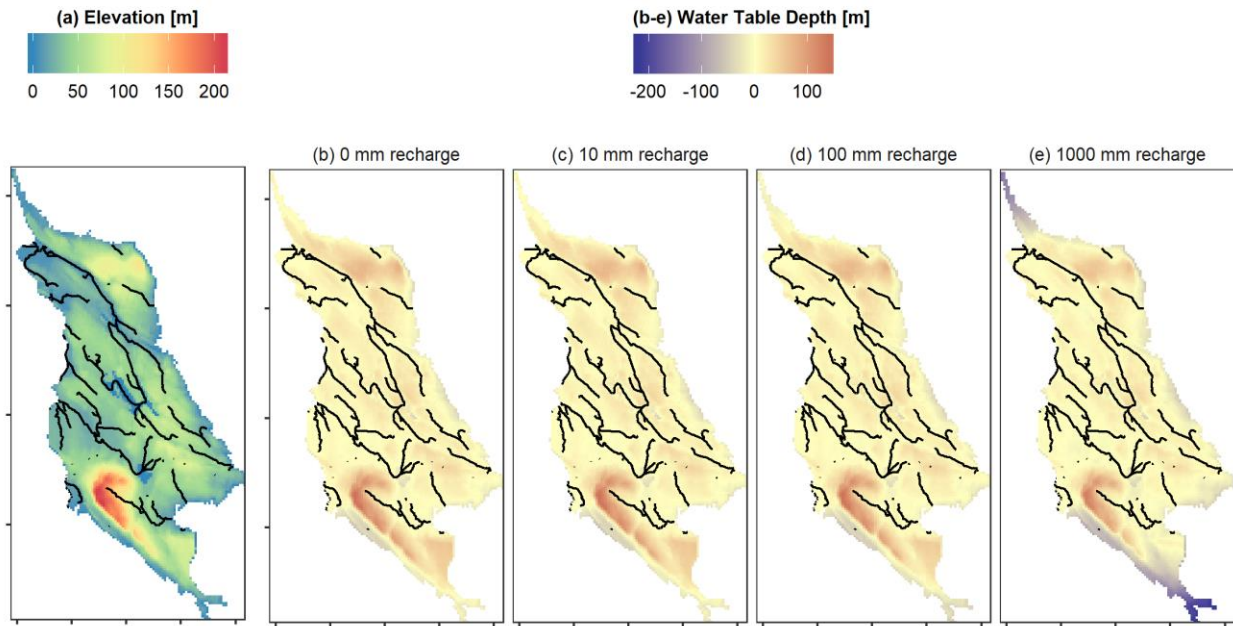
723
724
725
726
727

Figure S2. Performance of depletion apportionment equations based on stream reach length (left row) and distribution of stream reach lengths (right row) for (a-b) high, (c-d) medium, and (e-f) low drainage density domains.



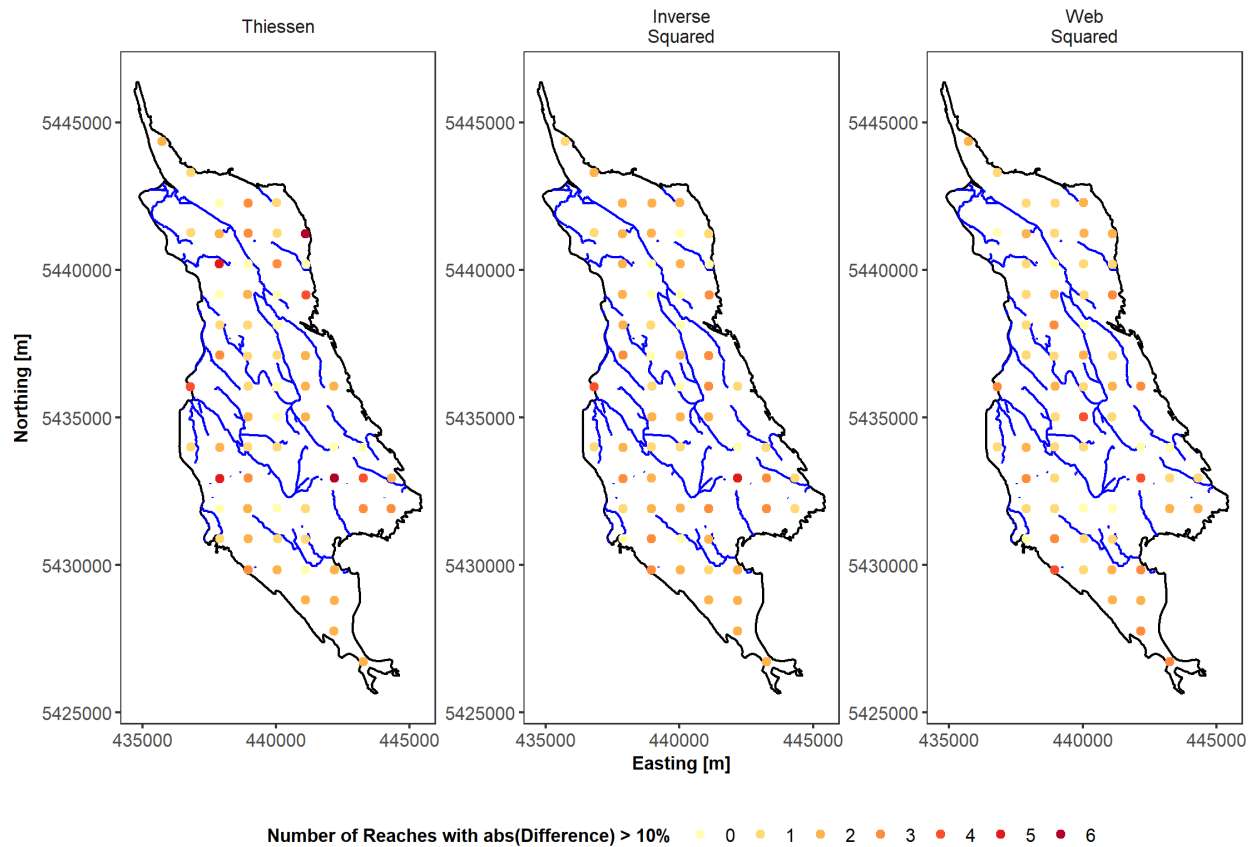
728
729
730

Figure S3. Contribution to overall MSE for different stream reach lengths across drainage densities and depletion attribution methods.



731
 732 **Figure S4.** (a) Ground surface elevation and water table depth with (b) 0, (c) 10, (d) 100, and (e) 1000
 733 mm yr⁻¹ groundwater recharge. Black lines show stream reaches.

734
 735



736
737
738

Figure S5. For each pumping well, the number of reaches with $> 10\%$ absolute difference between depletion apportionment equation and numerical model for the flat, low density domain.